Journal of Agricultural Sciences
(Tarim Bilimleri Dergisi)

J Agr Sci-Tarim Bili
e-ISSN: 2148-9297
jas.ankara.edu.tr

Identifying Agricultural Crops with Similar Spectral Properties Using Machine Learning Classifiers and SenseFly eBee SQ Multispectral UAV Images

Özlem Akar[a]*, Alper Akar[a], Halim Ferit Bayata[b]

[a]*Department of Architecture and City Planning, Erzincan Binali Yıldırım University, Erzincan, TÜRKIYE*

[b]*Department of Civil Engineering, Faculty of Engineering and Architecture, Erzincan Binali Yıldırım University, Erzincan, TÜRKIYE*

ARTICLE INFO

Research Article
Corresponding Author: Özlem Akar, E-mail: oakar@erzincan.edu.tr
Received: 13 February 2025 / Revised: 20 June 2025 / Accepted: 22 July 2025 / Online: 20 January 2026

Cite this article

Akar Ö, Akar A, Bayata H F (2026). Identifying Agricultural Crops with Similar Spectral Properties Using Machine Learning Classifiers and SenseFly eBee SQ Multispectral UAV Images. *Journal of Agricultural Sciences (Tarim Bilimleri Dergisi),* 32(1):93-111. DOI: 10.15832/ankutbd.1639091

ABSTRACT

This study investigates the use of vegetation indices for accurately identifying crops with similar spectral characteristics as grapes, apricots, tomatoes, wheat, and clover for enhancing crop monitoring and management. A 59-hectare area in Karakaya Village, located in the Üzümlü district of Erzincan Province, Türkiye, was selected as the study area. This area contains crops with varying textures, object height, and spectral characteristics. In the study, multispectral (MS) images were acquired using the SenseFly eBee SQ unmanned aerial vehicle (UAV), and subsequently processed to generate an orthophoto, digital terrain model (DTM), and digital surface model (DSM). Fifteen vegetation indices, Gabor texture features, and object heights were integrated into MS bands. Crop classification was performed using two high-accuracy machine learning algorithms: Random Forest (RF) and Support Vector Machine (SVM). According to the overall classification accuracy results, the use of vegetation indices improved classification accuracy by 9% for RF and 5% for SVM. Incorporating Gabor texture features with the top-performing indices (MACARI1, OSAVI, ADVI, and DVI) further increased accuracy to 20% for RF and 12% for SVM. Additionally, including object height alongside the indices and Gabor features resulted in further accuracy gains of 10% and 11% for RF and SVM, respectively. F1-score, specificity, and accuracy analyses, along with various kappa statistics, also the significant improvements in classification performance. According to the McNemar test, the χ^2 values comparing orthophoto images with those incorporating indices, texture, and object height ranged from 6.353 to 35.556 for RF, and from 7.220 to 11.021 for SVM. Since all χ^2 values exceeded 3.84, the results indicate statistically significant improvements in the classification accuracy at the 95% confidence interval.

Keywords: Spectral bands, Crop classification, Support vector machine, Random forest, Vegetation index, Gabor filter

1. Introduction

Agricultural crop classification plays a vital role in crop monitoring, management, and control within the agricultural sector (Potgieter et al. 2021; Tetteh et al. 2023; Deng et al. 2024). This importance stems from its ability to provide critical information on crop types and their spatial distribution. Furthermore, the accuracy of crop classification directly influences the effective of agricultural planning and decision-making processes (Zhang et al. 2016; Zhang et al. 2021a, Alzhanov & Nugumanova 2024). When agricultural crops are accurately classified, farmers can also determine which crops are best suited to specific areas, thereby improving overall productivity and efficiency (Yi et al. 2020; Devi & Kaur 2023). It also facilitates the more efficient use of agricultural inputs -such as water, fertilizers, and pesticides- resulting in cost savings and reduced environmental waste. Moreover, accurate classification helps determine optimal harvest times, minimizing post-harvest losses and maintaining crop quality (Peña-Barragán et al. 2011). In addition, classification support the development of effective marketing strategies by helping farmers and agricultural enterprises decide when and where to sell their products. It also enables early detection of crop diseases and pets, allowing for timely and targeted interventions (Lee et al. 2010; Domingues et al. 2022). Accurate classification further contributes to environmental sustainability by supporting soil conservation, maintaining water quality, preserving biodiversity, and aiding in climate change adaptation through a better understanding of crop-specific climatic requirement (Kumar et al. 2016). With advancements technology, Unmanned Aerial Vehicles (UAVs) and remote sensing have become increasingly popular tools in agricultural applications. These technologies allow for rapid and large-scale monitoring of agricultural fields, real-time data acquisition, and the provision of high spatial and spectral resolution imagery (Saleem et al. 2021; Moreno-Revelo et al. 2021; He et al. 2022; Faqe Ibrahim et al. 2023; Bareth & Hütt 2023).

Previous research on agricultural crop classification has demonstrated the extensive use of UAVs, satellite imagery, and vegetation indices. For instance, Kross et al. (2015) evaluated the contribution of vegetation indices derived from RapidEye satellite data to the estimation of leaf area index and biomass in corn and soybean fields. Maes & Steppe (2019) explored current

and future perspectives on the use of UAV use in precision agriculture, highlighting the role of vegetation indices in the monitoring crop health. Bendig et al. (2014) estimated barley biomass using crop surface models generated from UAV-based RGB imaging. Alzhanov & Nugumanova (2024) demonstrated the effectiveness of UAV multispectral images and gray level co-occurrence matrix (GLCM) texture features in crop classification. Zhang et al. (2023) integrated Sentinel-2 imagery with high-resolution UAV data to map rice yield potential during the planting season, demonstrating the effectiveness of modern imaging technologies in boosting agricultural productivity. Shahi et al. (2022) discussed how integrating UAV technology with machine learning enhances efficiency in the agriculture by monitoring plant health and stress, thereby improving overall crop management. Singh & Kumar (2023) emphasized the utility of remote sensing and vegetation indices in assessing vegetation health, reporting detailed classification accuracy across various land cover types such as mixed forest, scrub, grassland, riverine forest, cropland, settlements, dry riverbeds, and water bodies. Zhang et al. (2021b) applied multivariate regression methods using texture, color, and vegetation indices to predict wheat growth parameters from fixed-wing UAV imagery. Their work highlighted the potential of modern imaging technologies for assessing crop growth and development. Teimouri et al. (2023) proposed a cost-effective method for improving convolutional neural networks (CNN) based crop classification from satellite imagery by generating virtual training labels (VTL). Sah et al. (2023) monitored three stages of rice development using UAV-derived multispectral vegetation indices, emphasizing the potential applications of UAV imaging in rice farming. Wan et al. (2018) utilized UAVs equipped with RGB and multispectral cameras to estimate flower numbers in oilseed rape, applying vegetation indices and image classification techniques. Pipatsitee et al. (2023) examined the response of maize to water stress using various vegetation indices and UAV multispectral imagery. Song & Park (2020) investigated aquatic plant detection using multi-spectral UAV imaging and vegetation indices, focusing on the development of novel techniques for monitoring aquatic ecosystems. Feng et al. (2020) demonstrated the application of UAVs with multiple sensors in precision agriculture, particularly for cotton yield estimation. Wu et al. (2023) estimated chlorophyll content in spring wheat through multi-temporal UAV remote sensing, assessing plant physiological status overtime. Finally, Marcone et al. (2024) evaluated the use of random forest (RF) algorithm on UAV-acquired multispectral images to estimate garlic yield. By incorporating texture features, they significantly improved the accuracy of yield estimation models. This study highlighted UAV remote sensing as a fast and reliable tool for garlic yield monitoring. Collectively, these studies underscore the critical role and growing utility of UAV and remote sensing technologies in advancing agricultural monitoring, yield prediction, and crop management.

The literature review reveals that vegetation indices, texture features (e.g., GLCM), and spectral data are widely employed for crop monitoring, crop detection, crop health assessment, and management. However, no prior study has quantitatively assessed to extent to which the combined use of Gabor texture and object height information enhances discrimination of crops with nearly identical four-band UAV signatures under semi-arid Anatolian conditions. In contrast, the present study advances the field by integrating Gabor texture features and object height techniques previously reported to yield high classification accuracy (Akar & Güngör 2015; Akar & Tunc Gormus, 2021). These features are utilized in conjunction with machine learning algorithms to classify agricultural crops, thereby contributing to development of precision agriculture. Moreover, no comparable research has been conducted in Erzincan for these specific agricultural crops, which hold considerable economic importance for the region. Thus, the findings of this study are also expected to inform regional agricultural planning and policy development.

This study aims to compare the overall and per-class accuracies of Random Forest (RF) and Support Vector Machine (SVM) models for eight dominant crops in the Erzincan Plain, using multispectral imagery acquired by the SenseFly eBee SQ UAV and derived features. We hypothesize that augmenting multispectral data with vegetation indices, Gabor texture features, and object height information will improve overall classification accuracy by more than 10% compared to using multispectral data alone. To test this hypothesis, the study integrates supplementary data—including July 2022 orthomosaics, 15 vegetation indices, Gabor texture features, and object heights, all validated against 240 field polygons- with advanced machine learning techniques to generate highly accurate and reliable crop classification maps.

The methodological framework involves UAV-based image acquisition, photogrammetric processing to produce orthophoto and surface models, derivation of vegetation indices, texture metrics, and object height, and subsequent classification using Random Forest and SVM algorithms. Accuracy metrics such as F1-score, specificity, accuracy and kappa statistics are employed to assess classification performance, while McNemar's test is applied to determine the statistical significance of performance improvements across different feature sets. Figure 1 illustrates the methodology of the study.

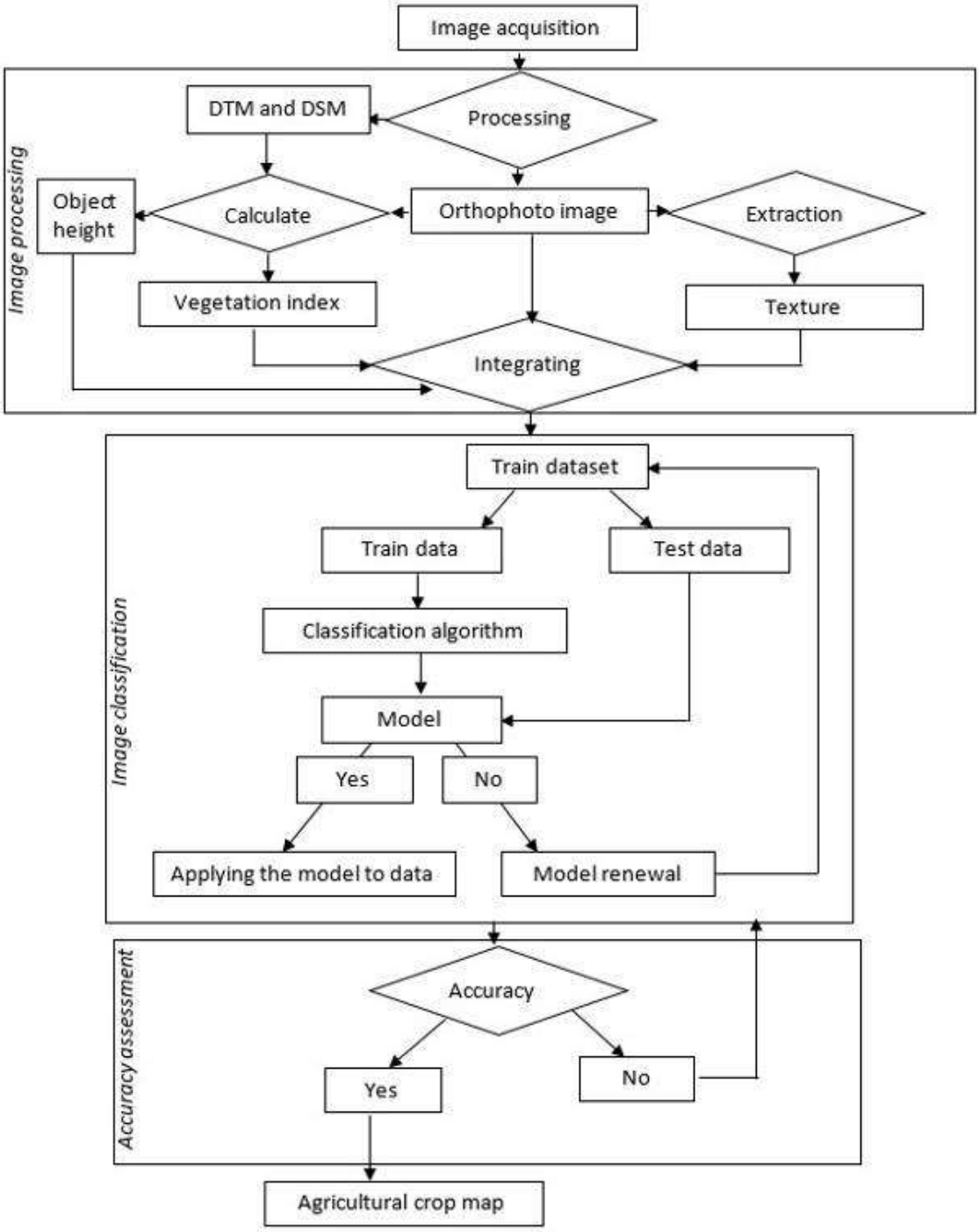

Figure 1- Workflow diagram

2. Material and Methods

2.1. Study area and dataset

The Erzincan Plain holds significant agricultural potential within the Eastern Anatolia Region (Hayli 2002). The region supports cultivation of various crops, including grapes, tomatoes, wheat, barley, apricots, apples, and pears. Notably, the grape variety grown in this area- patented as "Erzincan grape" by the Turkish Patent Institute in 2001 (TR Erzincan Governorate 2024)- is an endemic crop that plays a vital role in the local economy. Given its economic and ecological importance, the use of remote sensing technologies is essential for identifying suitable cultivation zones, expanding production area, and monitoring plant health disease outbreak effectively.

Karakaya Village, located in the Üzümlü district of Erzincan province, Türkiye, is characterized by a variety of agricultural crops -such as grapes, apricots, tomatoes, wheat- that exhibit diverse textures, heights, and spectral properties. These crops have

different planting periods throughout the year. Some, like apricot trees, are perennial and remain on the land permanently due to their tree woody structure. Therefore, this study aims to distinguish spectrally similar crops within a single growing season by incorporating additional data sources to enhance classification accuracy. For this reason, the region was selected as the study area (Figure 2). It covers approximately 59 hectares, and is located at approximately 39°40´45" N and 39°45´50" E.

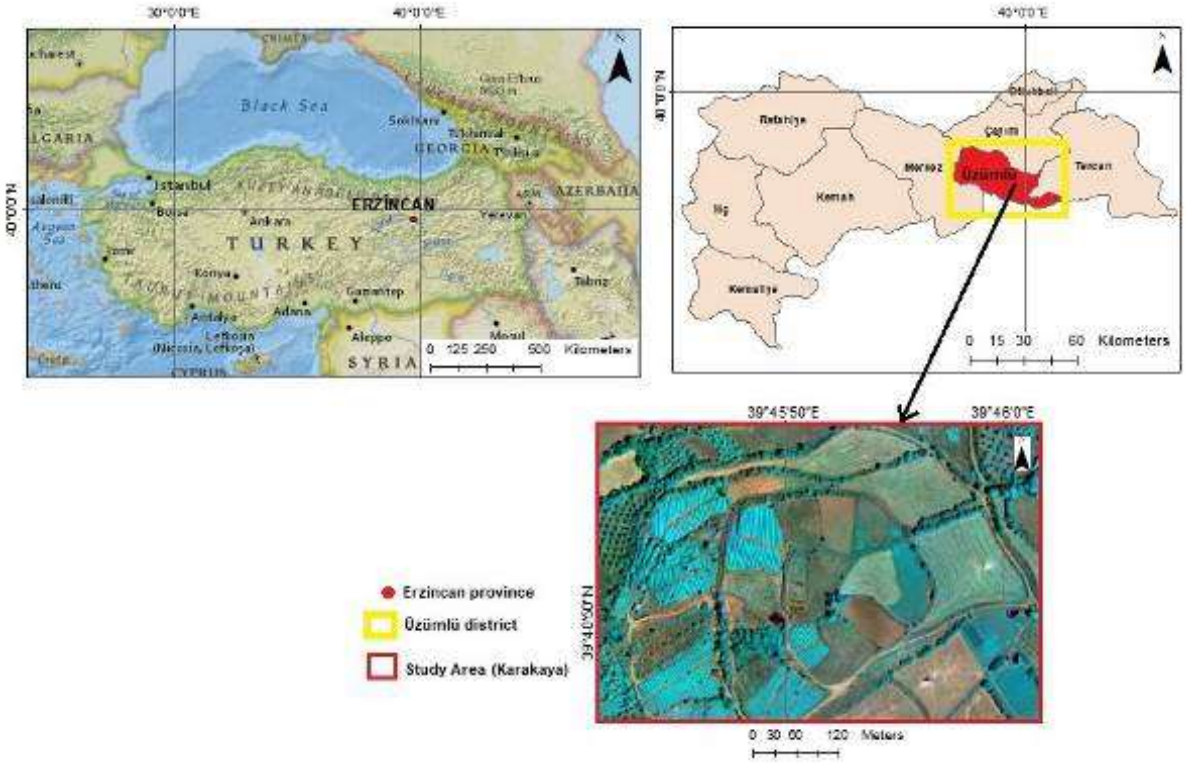

Figure 2- Study area

The study utilized images acquired from the SenseFly eBee SQ multispectral (MS) UAV. The SenseFly eBee SQ is regarded as one of the most efficient agricultural UAVs available on the market. It is equipped with Parrot's Sequoia camera, which features highly sensitive sensors capable of capturing 4-band multispectral imagery- Green (550nm), Red (660nm), Near Infrared (735nm), Red-edge (790nm)- as well as RGB imagery simultaneously. The multispectral sensor provides a resolution of 1.2 megapixels, while the RGB camera offers 16 megapixels. (SenseFly 2022)

The UAV flights were conducted in July 2022, coinciding with the phenological stage at which Erzincan grapes reaches maturity. This period was intentionally selected, as spectral and textural differences between crop types become most pronounced peak developmental stages. Grapevines, in particular, exhibit distinct spectral characteristics at maturity, this timing optimal optimal for accurate classification. According to the flight plan created using eMotion Ag software, at the UAV flew at an altitude of 116 meters for a total duration of 35 minutes. During the flight, 805 images were captured with 75% forward and side overlap, ensuring comprehensive coverage of the 59-hectare study area. The acquired images were processed in Pix4Dmapper software, resulting in a 16 cm/pixel (1xGSD) spatial resolution 4-band multispectral (MS) orthomosaics, along with a digital terrain model (DTM), and digital surface model (DSM) in the UTM WGS84 Zone 37 coordinate system. The Inverse Distance Weighting (IDW) algorithm was employed in the generation of this purpose. In the study, the MS bands were supplement with 15 different vegetation indices, Gabor texture features, and object height (derived from DSM-DTM subtraction), forming a comprehensive dataset for crop classification.

2.2. Vegetation indices

In the study, preferred total 15 vegetation indices commonly used in agricultural research were utilized. These include the Normalized Difference Vegetation Index (NDVI), Modified Simple Ratio (MSR1), Difference Vegetation Index (DVI), Optimized Soil Adjusted Vegetation Index (OSAVI), Modified Soil Adjusted Vegetation Index (MSAVI), Red edge Ratio Index 1 (RRI1), Red edge Ratio Index 2 (RRI2), Modified Chlorophyll Absorption in Reflectance Index (MACARI), Modified Chlorophyll Absorption in Reflectance Index 1 (MACARI1), Datts Index (Datts), Adjusted Difference Vegetation Index (aDVI), Green Normalized Difference Vegetation Index (GNDVI), Leaf Chlorophyll Index (LCI), Normalized Difference Red Edge (NDRE), Structure Intensive Pigment Index 2 (SIPI2). Details and formulations of these indices are presented in Table 1.

Table 1- Used vegetation index. The reflectance values in the table correspond to the GREEN, RED, RE, and NIR bands, representing green, red, red edge, and near infrared, respectively

Index	***Formula***	***Reference***
NDVI	$\left(\frac{NIR-RED}{NIR+RED}\right)$	Jordan1969; Pearson et al. 1972
MSR1	$\frac{\left(\frac{NIR}{RED-1}\right)}{\left(\sqrt{\left(\frac{NIR}{RED+1}\right)}\right)}$	Chen1996
DVI	$NIR-RED$	Jordan 1969
OSAVI	$(1+0.16)*\left(\frac{(NIR-RED)}{(NIR+RED+0.16)}\right)$	Rondeaux et al. 1996
MSAVI	$0.5*\left(2*NIR+1-\sqrt{(2*NIR+1)^2-8*(NIR-RED)}\right)$	Qi et al. 1994
RRI1	NIR/RE	Ehammer et al. 2010
RRI2	NIR/RED	Ehammer et al. 2010
MACARI	$\left((RE-RED)-0.2*(RE-GREEN)\right)*(\frac{RE}{RED})$	Daughtry et al. 2000
MACARI1	$1.2*(2.5*(NIR-RED)-1.3*(NIR-GREEN))$	Haboudane et al. 2004
Datts	$(NIR-RE)/(NIR-RED)$	Datt 1999
aDVI	$NIR-(\frac{GREEN+RED}{2})$	Broge & Leblanc 2001
GNDVI	$(NIR-GREEN)/(NIR+RED)$	Gitelson & Merzlyak 1997
LCI	$(NIR-RE)/(NIR+RED)$	Huete et al. 1994
NDRE	$(NIR-RE)/(NIR+RE)$	Sims et al. 2002
SIPI2	$(NIR-GREEN)/(NIR-RED)$	Penuelas et al. 1995

The indices were computed using Index Calculator module in Pix4Dmapper software. Spectral bands obtained from the multispectral imagery were used to calculate each index. The output of each index calculation was exported as a separate raster layer and subsequently used in classification.

2.3. Texture data and object height

In high spatial resolution images, such as that acquired by UAVs, pixel-based classifications are often affected by noise. To mitigate these effects and enhance performance, texture features are commonly integrated in to classification process (Kwak & Park 2019; Li et al. 2014). In this study, Gabor texture features were incorporated alongside vegetation indices for the classification of crops. The Gabor filter, which was found to provide high accuracy in our previous studies (Akar & Güngör 2015), was preferred. Gabor was first recognized as a windowed Fourier transform using the Gaussian distribution function as a window function (Debnath 2002). The most important feature of the Gabor filter is that it has optimal localization or resolution in both the spatial domain and the spatial-frequency domain. Additionally, since the Gabor filter can extract features similar to those perceived by the human visual system, it can play an effective role in classification applications (Hamamoto et al. 1998). The filter is defined by several parameters: lambda (λ), gamma (γ), angle (θ), phase (φ), and bandwidth (bw). According to these parameters, the Gabor filter is mathematically expressed by the following formula (Petkov & Wieling 2012);

$$\frac{\sigma}{\lambda}=\frac{1}{\pi}\sqrt{\frac{ln2}{2}}\frac{2^{bw}+1}{2^{bw}-1} \quad (1)$$

$$g_{\lambda,\theta,\varphi,\sigma,\gamma}(x,y)=exp\left(-\frac{x'^2+\gamma^2y'^2}{2\sigma^2}\right)cos(2\pi\frac{x'}{\lambda}+\varphi) \quad (2)$$

$$x'=xcos\theta+\mathrm{ysin}\theta \quad (3)$$

$$y'=-xsin\theta+\mathrm{ycos}\theta \quad (4)$$

Gamma (γ) and lambda (λ) determine the size of the filter. As the gamma value increases, the size of the filter decreases. Conversely, as lambda increases, sigma (σ) value also increases, resulting in a decrease in the gamma value. The bandwidth (bw) parameter plays an effective role in determining the σ value. Typically, the bandwidth is set to 1 (Petkov & Wieling 2012). For the image, texture extraction was performed by applying the Gabor filter using the optimal parameters ($\lambda=8, \gamma=1$) across eight orientation (θ):0°, 45°, 90°, 135°, 180°, 225°, 270°, and 315°. To enhance classification performance, the resulting Gabor incorporated as an additional band in to the dataset containing the highest-performing vegetation indices. The impact of this added texture information on classification performance was then evaluated.

Object height was utilized to distinguish crops that are similar spectral characteristics but differ in height and are located in close spatial proximity (e.g., grape and clover, apricot trees and grape, staked tomato and clover). In this study, object height was calculated by subtracting DTM from DSM (Formula 5) The resulting object height values were then incorporated in to the classification process, and their impact on classification performance was evaluated.

$$Object\ height = DTM - DTM \quad (5)$$

2.4. Machine learning algorithms

Pixel-based classification of the images was conducted using two machine learning methods-Random Forest (RF) and Support Vector Machine (SVM)- both of which are widely recognized in the literature for their high classification accuracy. The size of the classified image were 3033 x 2034 pixels. A total of eight classes were identified: grape, apricot, tomato, wheat, clover, forest, soil, and shadow. The training areas, comprising 2300–2900 pixels per class, were manually delineated through visual interpretation of the imagery using ENVI software. Special attention was given to ensure that the selected polygons contained spectrally homogeneous pixels to enhance classification accuracy. Additionally, training samples were spatially distributed across the study area to adequately represent the variability within each class. Shaded regions and spectrally heterogeneous areas were deliberately excluded to reduce noise and avoided potential misclassifications. The selected training areas were then exported to MATLAB R2018a, where a total of 19,499 training pixels were prepared using custom-developed code for training dataset. Two-thirds of these pixels were used for training, and one-third were reserved for testing. According to Breiman (2002), nearly optimal outcomes can be achieved by setting the number of variables (m) at each split to the square root of the total number of variables(M) (). Accordingly optimal parameters for Random Forest were determined as m=3 and N=200 trees. Figure 3 presents the accuracy results corresponding to the selected parameters. The images were classified in MATLAB software according to these optimal parameters. For the Support Vector Machine (SVM) classification, the Radial Based Function (RBF) kernel was employed. The optimal penalty parameter C was set to 100, with $gamma$ value of 0.25 for 4-bands and 0.20 for 5-bands. The same training data was used in ENVI software for SVM classification. Optimal parameters were identified by systematically testing various values and selecting those that yielded the highest classification accuracy.

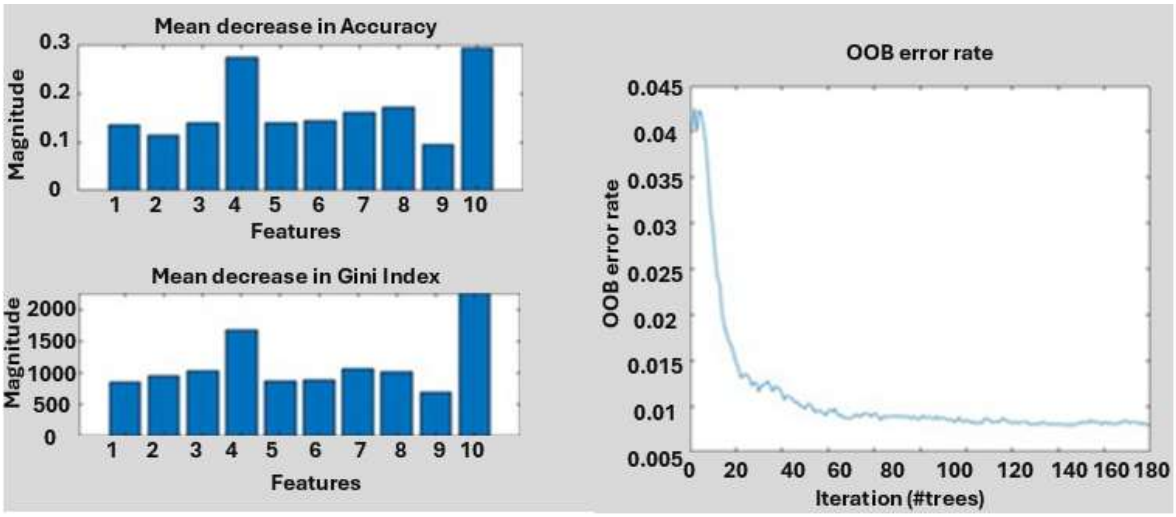

a) b)

Figure 3- Optimized hyper-parameters in each model for RF a) for m b) for N (Band(1-5): MS bands, bands(6-8): Vegetation index, band(9): Gabor features, Band(10): Object height)

2.4.1. Random forest

Random Forest (RF) classification is a widely used popular machine learning technique for regression and classification tasks (Akar & Güngör 2015; Akar & Tunc Gormus 2021; Gatera et al. 2023; Zermane et al. 2023; dos Santos et al. 2024; Iranzad & Liu 2024; Parashar et al. 2024). RF's success is based on the diversity and accuracy of its trees. Because it uses two well-known principles Random Subspaces and Bagging (Manzali & Elfar 2023). It is an ensemble learning method that generates a large number of decision trees during training and produces regression (average prediction of classes) or classification for each tree. The RF algorithm generates a large number of independent trees using a random vector sampled independently of the input vector, and each tree uses the majority vote received per class to classify an input vector (Breiman 1999). RF performs classification using the CART algorithm and GINI index as follows: A new training dataset T_k is generated from the training data T by resampling with replacement. A classifier $h(x, T_k)$ is then created using this new training dataset. Predictions from the classifier are aggregated by voting. For each x, y in the training data, only this classifier is used for voting. T_k does not include x and y (Breiman 2001). The parameters m (number of variables) and N (number of trees) specified by the user are considered in the development of the trees. A pixel is included in whichever class it is assigned to in most of the trees. However,

in RF, pruning is not performed as in the CART algorithm (Archer & Kimes 2008; Breiman 2001). Pal (2005) states that the choice of pruning method affects the performance of tree-based classifiers. The absence of pruning makes RF more preferable compared to other decision tree methods. (Rodriguez-Galiano et al. 2012). An increase in the GINI index shows an increase in node heterogeneity. A decrease in the GINI index shows an increase in node homogeneity. Branching is considered successful if the GINI index of a child node is less than the GINI index of a parent node. The tree branching process is completed when the GINI index reaches zero, i.e. when only one class remains at each leaf node (Watts et al. 2011).

2.4.2. Support vector machine

Support Vector Machines (SVM) is one of the powerful classification algorithm used in machine learning and statistics (Tzotsos & Argialas 2008; Awad & Khanna 2015; Kavitha & Kaulgud 2024). SVM developed by Vapnik (1998), aims to classify data points by determining a hyperplane or decision boundary that gives the best result in binary classification problems. Kernel and C values for the regulation's strength are the two parameters that are used (Yao et al. 2024). The following is the SVM's working principle:

1. Identification of the Hyperplane: SVM ascertains which hyperplane best divides the dataset. The plane that maximizes the margin between the two classes is known as the hyperplane (Figure 4).

2. Support Vector Selection: The data points (support vectors) that are closest to the hyperplane are found. By focusing on these areas, SVM optimizes the margin.

3. Optimization: SVM solves an optimization problem to determine which hyperplane offers the largest margin.

The objective function including the parameter C is expressed by formula (6)

$$\min\{\tfrac{1}{2}\|w\|^2 + C\sum_{i=1}^{n}\varepsilon_i\} \quad (6)$$

Accordingly, the primitive Langrange formula is expressed by formula 7 (Mather & Tso 2009).

$$L_{\text{primitive}} = \tfrac{1}{2}\|w\|^2 - \sum_{i=1}^{n}\alpha_i\,(y_i(w^T \times x_i + b) - 1 + \varepsilon_i) + C\sum_{i=1}^{n}\varepsilon_i - \sum_{i=1}^{n}\mu_i\varepsilon_i \quad (7)$$

4-Kernel Trics: To convert data into a higher dimensional space and make it linearly separable there in the event that it is not linearly separable, kernel tricks are employed.

$$K(x_i, x_j) = \phi(x_i)^T\phi(x_j) \quad (8)$$

Accordingly, the decision rule is expressed as follows (Mather & Tso 2009):

$$f(x) = sign\left(\sum_{i=1}^{nSV}\alpha_i\, y_i\phi(x_i).\phi(x_j) + b\right) \quad (9)$$

$$f(x) = sign\left(\sum_{i=1}^{nSV}\alpha_i\, y_i K(x_i, x_j) + b\right)$$

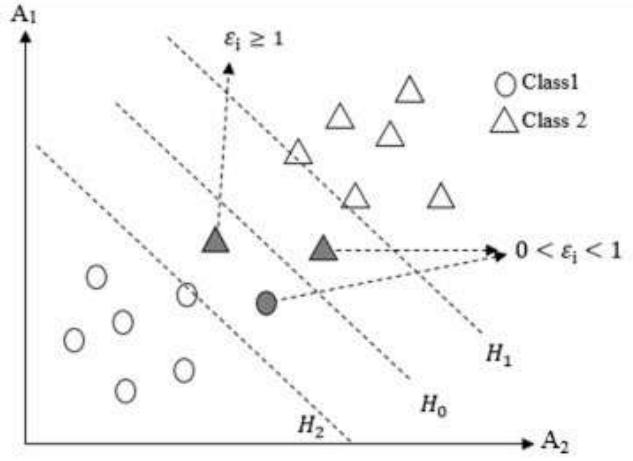

Figure 4- Principle of SVM

2.5. Accuracy assessment

The performance of classified images was evaluated using confusion matrix metrics, including overall accuracy (OA), Kappa coefficient, and the F1-score, which is calculated as the harmonic mean of user's accuracy (UA) and producer's accuracy (PA). Figure 5 presents the classified orthophoto image along with several thematic classified images with demonstrate good classification performance. The confusion matrix is one of the most commonly used post-classification accuracy analysis methods. Using this matrix, the relationships between the known reference data (ground truth) and the corresponding results obtained from the automatic classification can be categorically compared (Lillesand et al. 2004). In the study, the stratified randomization method was used to generate the confusion matrices with 30 validation points assigned to each class (Congalton & Green 1999; Congalton 2001; Mather 2004). Accordingly, a total of 240 reference points were generated for 8 classes analysed. These points were manually delineated based on visual interpretation of the orthophoto image. During sample selection, care was taken to ensure that the polygons consisted of spectrally homogeneous pixels and represented the spatial distribution of each class across the study area (Akar & Güngör 2012; Akar et al. 2021). The evaluation metrics derived from the confusion matrix –including precision (UA), recall (PA), F1-Score, specificity, and accuracy- are presented in Equations 10-14.

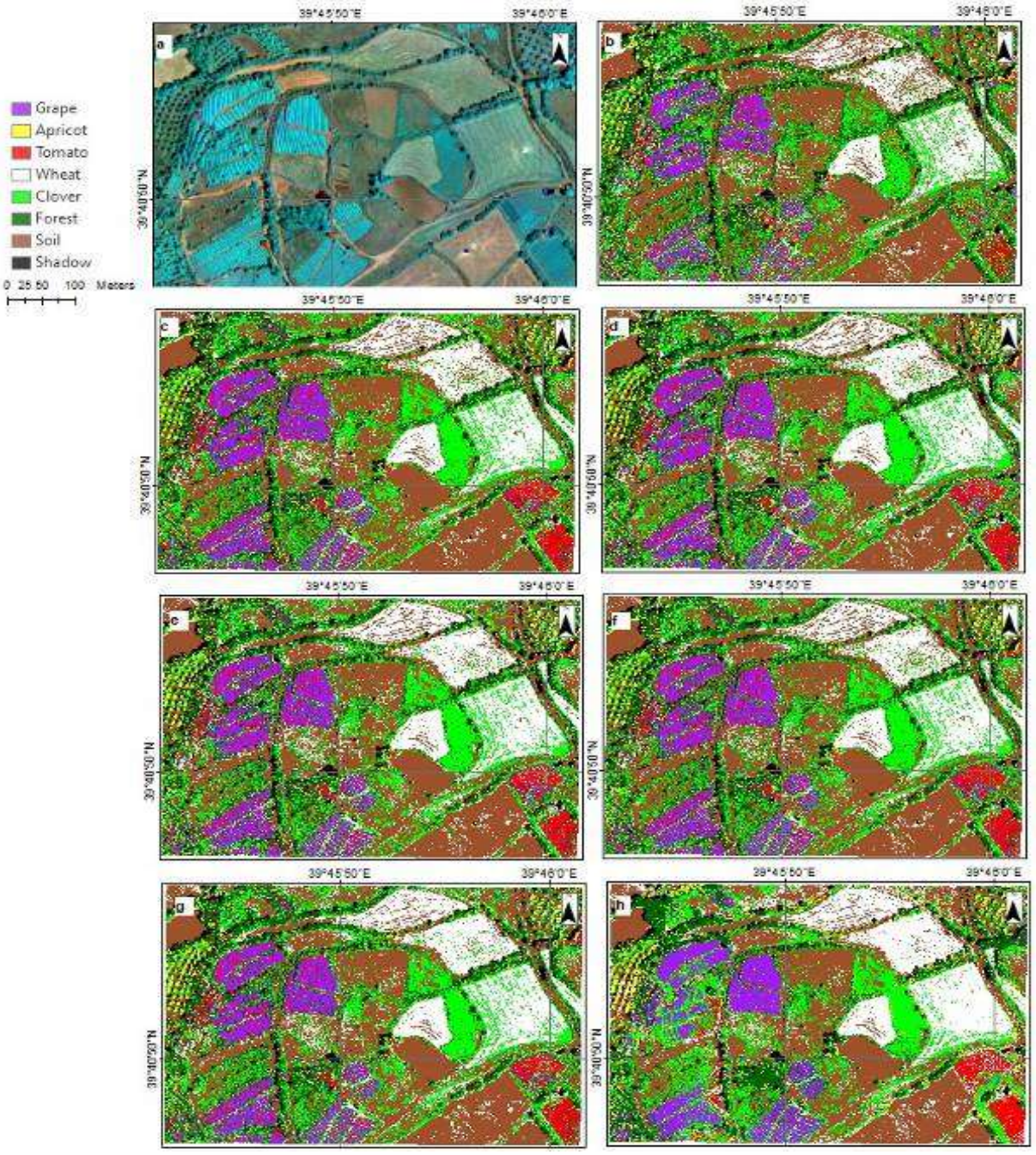

Figure 5- Thematic images classified a) Ortho (O), b) ortho+OSAVI+gabor (OOG), c) ortho+aDVI+gabor (OAG), d) ortho+DVI+gabor (ODG), e) ortho+MACARI1+gabor(OM1G), f) ortho+ MACARI1+ aDVI + DVI + OSAVI +gabor(OM1ADOG), h) ortho+ MACARI1+ aDVI + DVI + OSAVI +gabor +objheight(OM1ADOGH)

$$Precision = \frac{TP}{TP+FP} \quad (10)$$

$$Recall = \frac{TP}{TP+FN} \quad (11)$$

$$F1 - Score = \frac{2xPrecisionxRecall}{Precision+Recall} \quad (12)$$

$$Specificity = \frac{TN}{TN+FP} \quad (13)$$

$$Accuracy = \frac{TN+TP}{TN+TP+FP+FN} \quad (14)$$

Thus, in the confusion matrix, TP and TN stand for true positive and true negative observations, respectively. False positive and false negative observations are known as FP and FN (Amini et al. 2022). The metrics were computed for each class within confusion matrix generated be each classification method.

Another method for accuracy assessment is kappa (κ) analysis, which evaluates whether there is a statistically significant difference between two confusion matrices. A statistical evaluation of the degree of agreement between the used categories or classes and reference data is given by the κ value, which is computed between 0 and 1. Fit and classification accuracy are measured by this value, where higher values (approaching 1) indicate better alignment and accuracy and lower values (approaching 0) indicate poorer fit and lower classification accuracy. According to Pontius & Millones (2011), Kappa has come under fire for trying to evaluate accuracy to a randomized baseline. They suggested, instead, making use of allocation and quantity disagreements, which draw attention to the differences between a comparison map and a reference map. Whereas allocation disagreement deals with variations in the spatial distribution of categories between the reference and comparison maps, quantity disagreement concentrates on discrepancies in category proportions between the reference and comparison maps (Akar 2022). This recommendation led to the computation of allocation and quantity values for each image's post-classification accuracy evaluation, along with the kappa coefficient. The McNemar test was then used to determine whether or not there were statistically significant differences. This nonparametric test enables pairwise comparison of classification outcomes generated by different algorithms. The McNemar test was computed using the formula (15) (Foody 2004).

$$\chi^2 = \frac{(|f_{12}-f_{21}|-1)^2}{f_{12}+f_{21}} \quad (15)$$

Where: f_{12} represents the number of pixels that the second approach incorrectly classified but the first method properly classified, and f_{21} represents the number of pixels that the first method incorrectly classified but the second method correctly classified.

3. Results and Discussion

The overall classification accuracies derived from the confusion matrices are presented in Table 2. The Integration of vegetation indices, texture and object height improved OA from 0.74 to 0.94 with RF and from 0.70 to 0.91 with SVM. Kwak and Park (2019) reported that incorporating texture features is more effective than using multi-temporal images for improving classification accuracy in single-date images. Their study demonstrated an 8% in accuracy with the combined use texture and spectral information. Similarly, Lucena et al. (2022) achived a 7% improvement using DTM and spectral information, while Atik (2025) reported a 7% gain when DTM, spectral information and vegetation indices were used combination. The finding of the present study are consistent with these conclusions. Specifically, the inclusion of vegetation indices resulted in a 9% improvement in RF and 5% improvement in SVM. The addition Gabor texture features- along with vegetation indices like MACARI1, OSAVI, ADVI, and DVI- further enhanced classification performance, leading to gains of 20% in RF and 12% in SVM. Moreover, incorporating object height information in addition to indices and texture features, let to an additional improvement of 10% for RF and 11% for SVM, compared to classification based solely on orthophoto imagery.

Table 2- Overall accuracy for RF and SVM

Image	*RF*	*SVM*
Ortho (O)	73.75	68.75
ortho+LCI	71.25	70.83
ortho+NDRE	72.5	69.17
ortho+SIPI2	73.33	69.17
ortho+Datts	74.17	69.17
ortho+RRI1	74.17	73.33
ortho+RRI2	74.17	74.17
ortho+GNDVI	74.58	73.33
ortho+NDVI	75.42	73.33
ortho+MRS1	76.25	73.33
ortho+MSAVI	79.58	72.08
ortho+MACARI	80	71.67
ortho+OSAVI	80	73.75
ortho+aDVI	80.42	72.5
ortho+DVI	81.25	72.08
ortho+MACARI1	82.92	74.17
ortho+MACARI+gabor (OMG)	88.75	80.83
ortho+OSAVI+gabor (OOG)	93.33	79.58
ortho+aDVI+gabor (OAG)	93.33	78.75
ortho+DVI+gabor (ODG)	93.33	80.42
ortho+MACARI1+gabor(OM1G)	93.75	80.83
ortho+ MACARI1+ aDVI + DVI + OSAVI +gabor(OM1ADOG)	90.42	80.42
ortho+ MACARI1+ aDVI + DVI + OSAVI +gabor +objheight(OM1ADOGH)	83.33	80

PA values for RF, presented in Table 3, indicated the highest performance for the grape class using the OOG (ortho+OSAVI+gabor) and OM1G (ortho+MACARI1+gabor) dataset, with an improvement ranging from 17% to 20%. In the apricot class, the OM1G dataset achieved the highest classification accuracy at 43% by OOG at 39%, by OMG (ortho+MACARI+gabor) and OM1ADOG (ortho+ MACARI1+ aDVI + DVI + OSAVI +gabor) at 30%, by OAG (ortho+aDVI+gabor) and ODG (ortho+DVI+gabor) at 35%, and by OM1ADOGH (ortho+ MACARI1+ aDVI + DVI + OSAVI +gabor +objheight) at 26%. For tomato class, classification accuracy improved significantly, with increases ranging from 65% to 70%, while the wheat class exhibited a maximum improvement of 14%."In the clover class, OOG achieved a PA of 22% and additional improvements were observed with OMG (6%), OAG(17%), ODG(19%), OM1G (17%), and OM1ADOG(17%). The forest class were more accurately classified using OMG (6%), OOG (11%), OAG (17%), ODG (14%), OM1G (14%), and OM1ADOG (11%). The soil class showed the highest improvement with OAG at 17%, while the shadow class, OMG and ODG yielded of the greatest increases, both at 11%.

Table 3- Producer's and User's Accuracies for RF

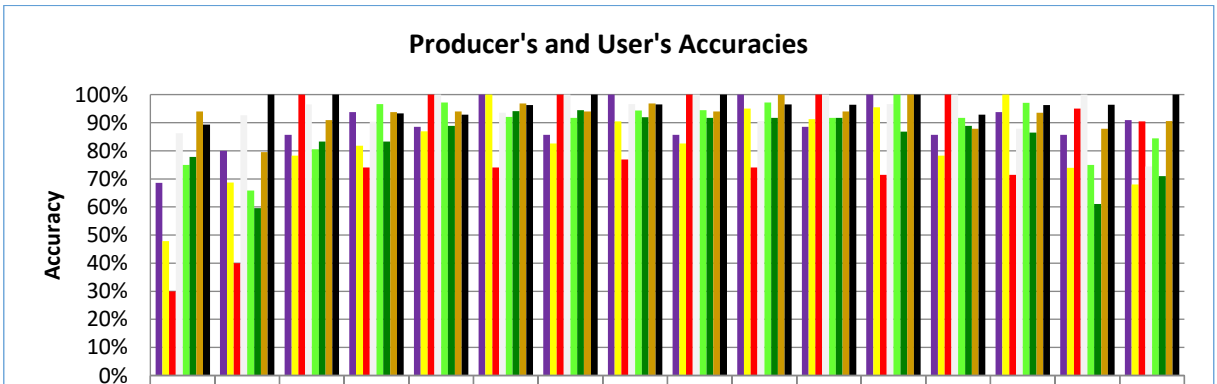

	O		OMG		OOG		OAG		ODG		OM1G		OM1ADOG		OM1ADOGH	
	PA (%)	UA (%)	PA (%)	UA (%)	PA (%)	UA (%)	PA (%)	UA (%)	PA (%)	UA (%)	PA (%)	UA (%)	PA (%)	UA (%)	PA (%)	UA (%)
Grape	68.57	80.00	85.71	93.75	88.57	100.0	85.71	100.0	85.71	100.0	88.57	100.0	85.71	93.75	85.71	90.91
Apricot	47.83	68.75	78.26	81.82	86.96	100.0	82.61	90.48	82.61	95.00	91.30	95.45	78.26	100.0	73.91	68.00
Tomato	30.00	40.00	100.0	74.07	100.0	74.07	100.0	76.92	100.0	74.07	100.0	71.43	100.0	71.43	95.00	90.48
Wheat	86.21	92.59	96.55	90.32	100.0	93.55	100.0	96.67	100.0	90.63	100.0	96.67	100.0	87.88	100.0	74.36
Clover	75.00	65.85	80.56	96.67	97.22	92.11	91.67	94.29	94.44	97.14	91.67	100.0	91.67	97.06	75.00	84.38
Forest	77.78	59.57	83.33	83.33	88.89	94.12	94.44	91.89	91.67	91.67	91.67	86.84	88.89	86.49	61.11	70.97
Soil	93.94	79.49	90.91	93.75	93.94	96.88	93.94	96.88	93.94	100.0	93.94	100.0	87.88	93.55	87.88	90.63
Shadow	89.29	100.0	100.0	93.33	92.86	96.30	100.0	96.55	100.0	96.55	96.43	100.0	92.86	96.30	96.43	100.0

Regarding UA, the addition of vegetation indices, Gabor texture features and object height let to improvements ranging from 11% to 20% for grape class, 13% to 31%for the apricot class and 14% to 50%for the tomato class. For the clover class UA increased by 31% to 34%. The forest class was best represented by OAG and ODG, both achieving 32%, while the soil class showed the highest UA with ODG and OM1G, both at 21%.

When examining the PA (Producer's Accuracy) and UA (User's Accuracy) accuracies in SVM (Table 4), similar results to the RF classifier were observed. PA increased for the grape by ≤ 29 %, for the apricot by 4%-17%, for the tomato by ≤ 65%, for the wheat by ≤ 3 %, for the clover by ≤ 6%. UA raised for the grape by ≤ 19 %, for the apricot by 8%-17%, for the tomato by 33%-54%, for the wheat by ≤ 7 %, for the clover by 32%-39%. Furthermore, an examining of the confusion matrices revealed that due to the similarities in spectral characteristics, the clover class was often frequently misclassified as grape, apricot, forest, and soil. The Wheat class was commonly confused with clover, while the forest class was misclassified as grape, apricot, and clover. The misclassifications can be attributed particularly to the similarities in texture, object height, and spectral characteristics between forest and apricot trees reduced classification accuracy.

Table 4- Producer's and User's Accuracies for SVM

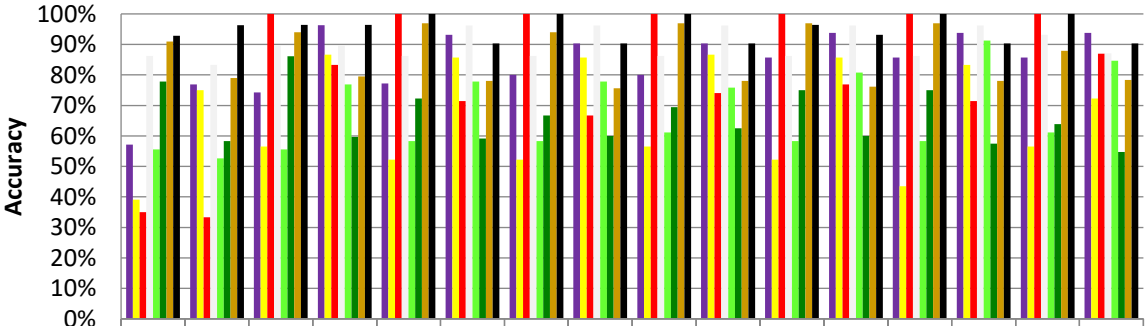

	O		OMG		OOG		OAG		ODG		OM1G		OM1ADOG		OM1ADOGH	
	PA (%)	UA (%)	PA (%)	UA (%)	PA (%)	UA (%)	PA (%)	UA (%)	PA (%)	UA (%)	PA (%)	UA (%)	PA (%)	UA (%)	PA (%)	UA (%)
Grape	57.14	76.92	74.29	96.30	77.14	93.10	80.00	90.32	80.00	90.32	85.71	93.75	85.71	93.75	85.71	93.75
Apricot	39.13	75.00	56.52	86.67	52.17	85.71	52.17	85.71	56.52	86.67	52.17	85.71	43.48	83.33	56.52	72.22
Tomato	35.00	33.33	100.0	83.33	100.0	71.43	100.0	66.67	100.0	74.07	100.0	76.92	100.0	71.43	100.0	86.96
Wheat	86.21	83.33	89.66	89.66	86.21	96.15	86.21	96.15	86.21	96.15	86.21	96.15	86.21	96.15	93.10	87.10
Clover	55.56	52.63	55.56	76.92	58.33	77.78	58.33	77.78	61.11	75.86	58.33	80.77	58.33	91.30	61.11	84.62
Forest	77.78	58.33	86.11	59.62	72.22	59.09	66.67	60.00	69.44	62.50	75.00	60.00	75.00	57.45	63.89	54.76
Soil	90.91	78.95	93.94	79.49	96.97	78.05	93.94	75.61	96.97	78.05	96.97	76.19	96.97	78.05	87.88	78.38
Shadow	92.86	96.30	96.43	96.43	100.0	90.32	100.0	90.32	100.0	90.32	96.43	93.10	100.0	90.32	100.0	90.32

Nidamanuri (2024), Rissanen et al. (2019), and Pun Magar et al. (2025) utilized multi-temporal imagery based on crop planting times to improve classification. They generated pre-planting DTM and post-planting DSM data to calculate object height. In contrast, Kwak and Park (2019) emphasized the importance of using ancillary data to enhance classification accuracy when using single-date imagery. Building upon these findings, the present study investigated the contribution of object height to improved classification accuracy. As evident from these results, integrating Gabor texture features, vegetation indices, and object height into the 4-band orthophoto imagery significantly improved the discrimination between grape and tomato crops. Specifically, for tomatoes, classification accuracy increased by 31% to 70% with both RF and SVM. For grapes, RF achieved improvements of 17% in PA and 11% in UA, while SVM showed increases of 29% (PA) and 17% (UA). The findings demonstrate that crops with similar spectral characteristics but differing in structural attributes (e.g. height) and located in close spatial proximity- such as grape and clover, apricot trees and grape, staked tomato and clover- can be more effectively distinguished using combination of object height and texture information.

According to the F1-score, specificity, and accuracy analyses for the Random Forest (RF) classifier, it is evident in Table 5 that the inclusion of vegetation indices, Gabor texture features, and object height significantly contributed to classification performance. For RF (minimum and maximum values), the F1-score improved from 0.34–0.95 to 0.65–0.97. Specificity increased from 0.89–1.00 to 0.94–1.00, and accuracy improved from 0.87–0.98 to 0.90–1.00. Similarly, when examining Table 6 for Support Vector Machines (SVM), the F1-score increased from 0.34–0.95 to 0.63–0.96. Specificity improved from 0.87–0.99 to 0.94–0.99, and accuracy increased from 0.83–0.98 to 0.91–0.99.

When evaluating F1-score improvements on a per-class basis for the RF classifier, the following increases were observed: the grape (20%), apricot (37%), tomato (58%), wheat (9%), clover (26%), forest (26%), soil (11%), and shadow (4%). For SVM (Table 6), corresponding increases were recorded asF1-score increases were recorded as: 24%, 12%, 59%, 6%, 17%, 4%, 2%, and 2%, respectively. The most significant notable gains were seen in the apricot and staked tomato classes. Despite their spectral similarity to neighboring classes, these crops were successfully distinguished due to their unique texture and height characteristics. Specificity improvements ranged from 1% to 10%, while accuracy increased between by 1% to 11% for RF and 1% to 13% for SVM, indicating enhanced class discrimination. The results particularly underscore the crucial role of object height with the staked tomato class exhibiting a remarkable 58%- 59% increase in the F1-score.

Table 5- F1-score, specificity, and accuracy analyses for RF

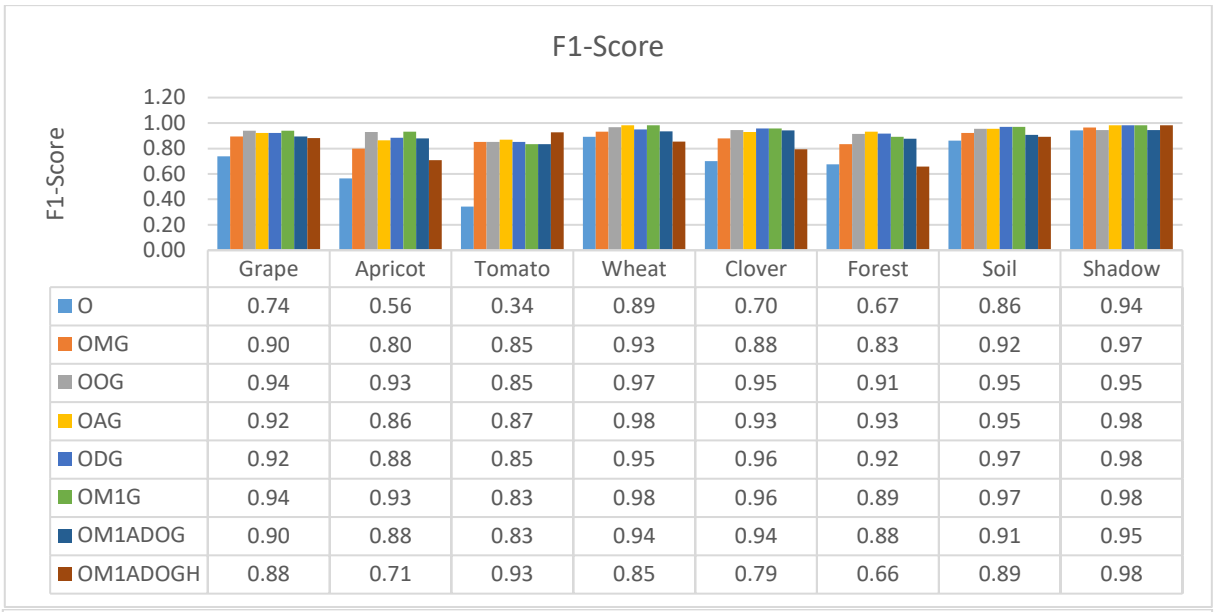

	Grape	Apricot	Tomato	Wheat	Clover	Forest	Soil	Shadow
O	0.74	0.56	0.34	0.89	0.70	0.67	0.86	0.94
OMG	0.90	0.80	0.85	0.93	0.88	0.83	0.92	0.97
OOG	0.94	0.93	0.85	0.97	0.95	0.91	0.95	0.95
OAG	0.92	0.86	0.87	0.98	0.93	0.93	0.95	0.98
ODG	0.92	0.88	0.85	0.95	0.96	0.92	0.97	0.98
OM1G	0.94	0.93	0.83	0.98	0.96	0.89	0.97	0.98
OM1ADOG	0.90	0.88	0.83	0.94	0.94	0.88	0.91	0.95
OM1ADOGH	0.88	0.71	0.93	0.85	0.79	0.66	0.89	0.98

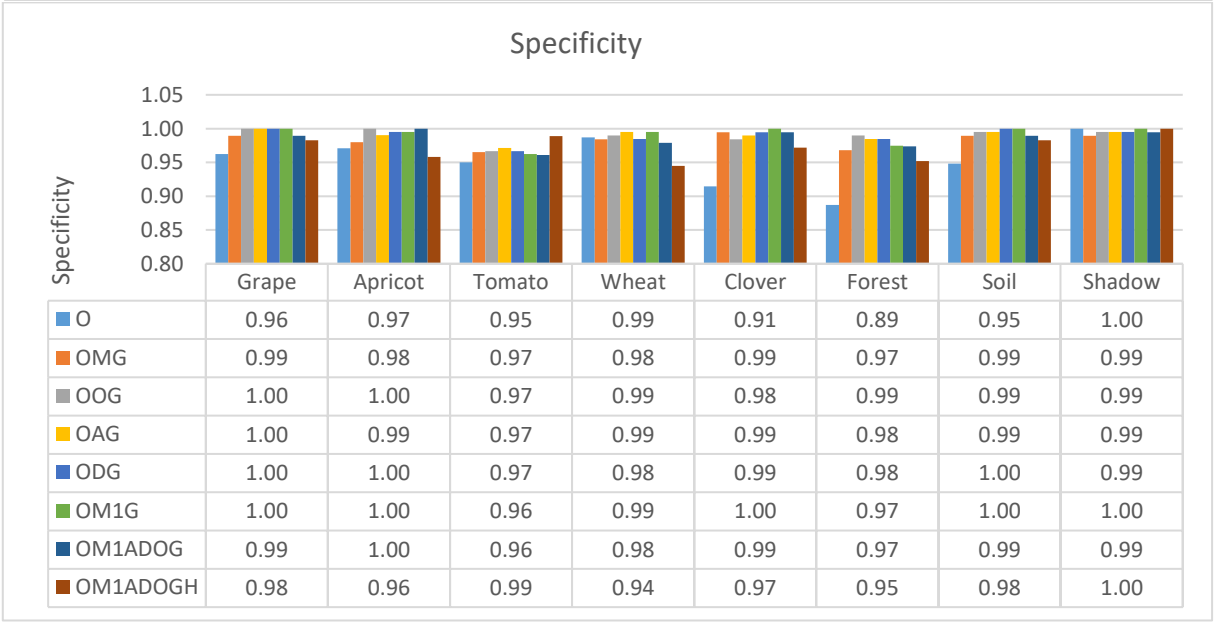

	Grape	Apricot	Tomato	Wheat	Clover	Forest	Soil	Shadow
O	0.96	0.97	0.95	0.99	0.91	0.89	0.95	1.00
OMG	0.99	0.98	0.97	0.98	0.99	0.97	0.99	0.99
OOG	1.00	1.00	0.97	0.99	0.98	0.99	0.99	0.99
OAG	1.00	0.99	0.97	0.99	0.99	0.98	0.99	0.99
ODG	1.00	1.00	0.97	0.98	0.99	0.98	1.00	0.99
OM1G	1.00	1.00	0.96	0.99	1.00	0.97	1.00	1.00
OM1ADOG	0.99	1.00	0.96	0.98	0.99	0.97	0.99	0.99
OM1ADOGH	0.98	0.96	0.99	0.94	0.97	0.95	0.98	1.00

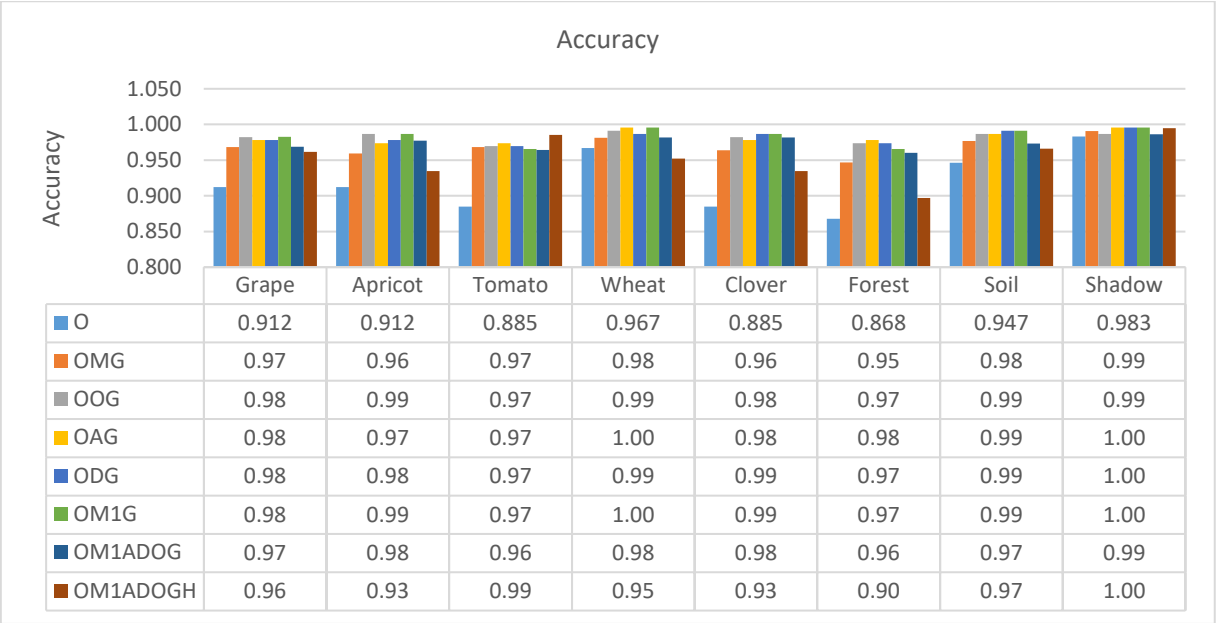

	Grape	Apricot	Tomato	Wheat	Clover	Forest	Soil	Shadow
O	0.912	0.912	0.885	0.967	0.885	0.868	0.947	0.983
OMG	0.97	0.96	0.97	0.98	0.96	0.95	0.98	0.99
OOG	0.98	0.99	0.97	0.99	0.98	0.97	0.99	0.99
OAG	0.98	0.97	0.97	1.00	0.98	0.98	0.99	1.00
ODG	0.98	0.98	0.97	0.99	0.99	0.97	0.99	1.00
OM1G	0.98	0.99	0.97	1.00	0.99	0.97	0.99	1.00
OM1ADOG	0.97	0.98	0.96	0.98	0.98	0.96	0.97	0.99
OM1ADOGH	0.96	0.93	0.99	0.95	0.93	0.90	0.97	1.00

Table 6- F1-score, specificity, and accuracy analyses for SVM

	Grape	Apricot	Tomato	Wheat	Clover	Forest	Soil	Shadow
O	0.66	0.51	0.34	0.85	0.54	0.67	0.85	0.95
OMG	0.84	0.68	0.91	0.90	0.65	0.70	0.86	0.96
OOG	0.84	0.65	0.83	0.91	0.67	0.65	0.86	0.95
OAG	0.85	0.65	0.80	0.91	0.67	0.63	0.84	0.95
ODG	0.85	0.68	0.85	0.91	0.68	0.66	0.86	0.95
OM1G	0.90	0.65	0.87	0.91	0.68	0.67	0.85	0.95
OM1ADOG	0.90	0.57	0.83	0.91	0.71	0.65	0.86	0.95
OM1ADOGH	0.90	0.63	0.93	0.90	0.71	0.59	0.83	0.95

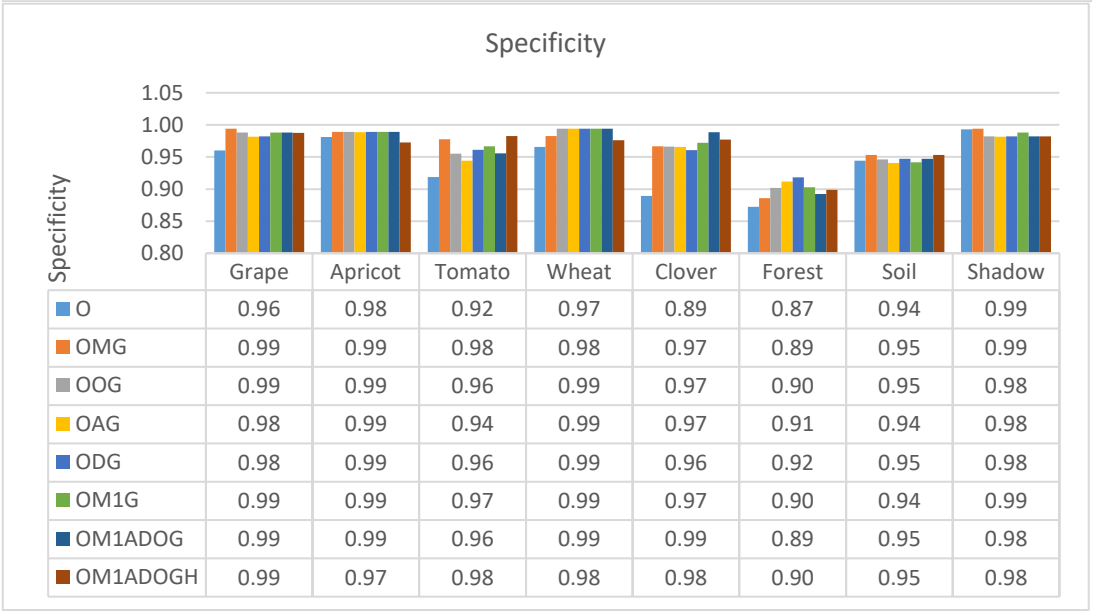

	Grape	Apricot	Tomato	Wheat	Clover	Forest	Soil	Shadow
O	0.96	0.98	0.92	0.97	0.89	0.87	0.94	0.99
OMG	0.99	0.99	0.98	0.98	0.97	0.89	0.95	0.99
OOG	0.99	0.99	0.96	0.99	0.97	0.90	0.95	0.98
OAG	0.98	0.99	0.94	0.99	0.97	0.91	0.94	0.98
ODG	0.98	0.99	0.96	0.99	0.96	0.92	0.95	0.98
OM1G	0.99	0.99	0.97	0.99	0.97	0.90	0.94	0.99
OM1ADOG	0.99	0.99	0.96	0.99	0.99	0.89	0.95	0.98
OM1ADOGH	0.99	0.97	0.98	0.98	0.98	0.90	0.95	0.98

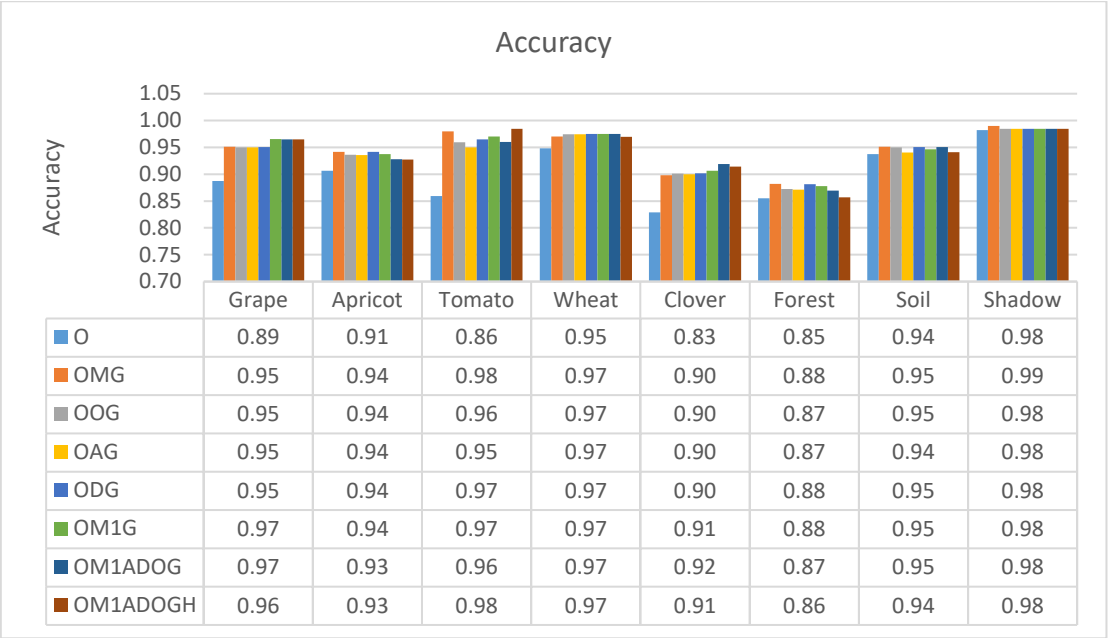

	Grape	Apricot	Tomato	Wheat	Clover	Forest	Soil	Shadow
O	0.89	0.91	0.86	0.95	0.83	0.85	0.94	0.98
OMG	0.95	0.94	0.98	0.97	0.90	0.88	0.95	0.99
OOG	0.95	0.94	0.96	0.97	0.90	0.87	0.95	0.98
OAG	0.95	0.94	0.95	0.97	0.90	0.87	0.94	0.98
ODG	0.95	0.94	0.97	0.97	0.90	0.88	0.95	0.98
OM1G	0.97	0.94	0.97	0.97	0.91	0.88	0.95	0.98
OM1ADOG	0.97	0.93	0.96	0.97	0.92	0.87	0.95	0.98
OM1ADOGH	0.96	0.93	0.98	0.97	0.91	0.86	0.94	0.98

Moreover, these findings highlight benefits of integrating object height information when classifying spectral similar but structurally district crops. The inclusion of Gabor texture features alongside vegetation indices further contributed to improved classification performance across multiple crop types.

As presented in Table 7, the $\kappa_{allocation}$, $\kappa_{quantity}$, κ_{histo} and $\kappa_{cohen's}$ kappa values for the orthophoto image using RF classifier were 0.78, 0.83, 0.89, and 0.74, respectively. In contrast, the OM1G, which yielded the highest classification accuracy, achieved corresponding kappa values of 0.98, 0.91, 0.95, and 0.94. Compared to the orthophoto image, OM1G showed substantial improvements of 20% in $\kappa_{allocation}$, 8% in $\kappa_{quantity}$,6 % in κ_{histo},and20% in $\kappa_{cohen's}$. Similarly, for OM1ADOGH, the $\kappa_{allocation}$, $\kappa_{quantity}$, κ_{histo} and $\kappa_{cohen's}$ kappa values were 0.86, 0.89, 0.94, and 0.83 for RF, and 0.84, 0.85, 0.91, and 0.80 for SVM, respectively. These results clearly demonstrate that the integration of vegetation indices, Gabor texture features, and object height significantly enhanced classification performance when combined orthophoto imagery

Table 7- Kappa analysis for RF and SVM

RF	O	OMG	OOG	OAG	ODG	OM1G	OM1ADOG	OM1ADOGH
OVERALL ACCURACY	0.74	0.89	0.93	0.93	0.93	93.75	0.90	0.83
$\kappa_{allocation}$	0.78	0.92	0.97	0.97	0.97	0.98	0.95	0.86
$\kappa_{quantity}$	0.83	0.91	0.91	0.93	0.91	0.91	0.89	0.89
κ_{histo}	0.89	0.95	0.95	0.96	0.95	0.95	0.94	0.94
$\kappa_{cohen's}$	0.74	0.89	0.93	0.93	0.93	0.94	0.90	0.83

SVM	O	OMG	OOG	OAG	ODG	OM1G	OM1ADOG	OM1ADOGH
Overall accuracy	0.69	0.81	0.80	0.79	0.80	0.81	0.80	0.80
$\kappa_{allocation}$	0.71	0.89	0.88	0.86	0.87	0.89	0.91	0.84
$\kappa_{quantity}$	0.84	0.79	0.78	0.80	0.82	0.80	0.75	0.85
κ_{histo}	0.90	0.88	0.87	0.88	0.89	0.88	0.86	0.91
$\kappa_{cohen's}$	0.69	0.81	0.79	0.78	0.80	0.81	0.80	0.80

To determine the statistical significance of differences between classification results, the McNemar test was applied (Table 8). For RF,χ^2 values ranged from 6.353 to 35.556, while for SVM, values ranged from 7.220 to 11.021. Since all computed χ^2values exceeded the critical threshold of 3.84, the results confirmed statistically significant improvements in classification accuracy at a 95% confidence interval. The final thematic crop map is presented in Figure 6.

Table 8- McNemar test analysis

RF

		f_{11}	f_{12}	f_{21}	f_{22}	χ^2
O	OMG	181	9	38	12	16.681
	OOG	188	2	43	7	35.556
	OAG	185	5	43	7	28.521
	ODG	185	5	43	7	28.521
	OM1ADOG	184	6	41	9	24.596
	OM1ADOGH	174	16	35	15	6.353
	OM1G	185	5	45	5	30.420

SVM

		f_{11}	f_{12}	f_{21}	f_{22}	χ^2
O	OMG	168	12	35	25	10.298
	OOG	165	15	35	25	7.220
	OAG	166	14	35	25	8.163
	ODG	166	14	37	23	9.490
	OM1ADOG	166	14	35	25	8.163
	OM1ADOGH	164	16	38	22	8.167
	OM1G	168	12	36	24	11.021

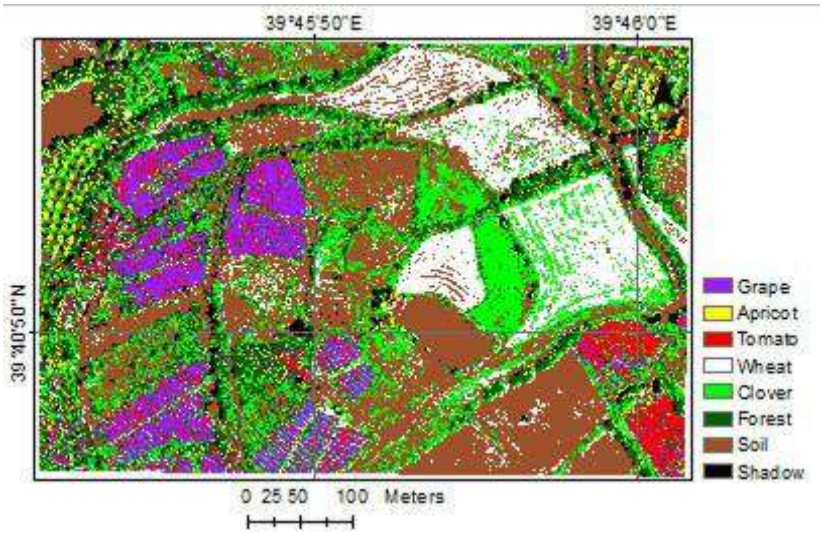

Figure 6- Thematic crop map

4.Conclusions

Accurate classification of agricultural crops is avital application that contributes significantly to the agricultural sector in numerous ways, including improving productivity environmental sustainability, aiding in disease control, and supporting economic development. Effective crop mapping is essential for informed decision-marking in agricultural policies, as well as for the monitoring and management agricultural activities. Recent studies by Pei et al. (2024), Xu et al. (2022) and Zou et al. (2024) emphasized that the combined use of vegetation indices and texture information can enhanced model accuracy. Building upon this, the present study employed MS bands captured by the SenseFly eBee SQ agricultural drone, along with various vegetation indices, Gabor texture features, and object height data. The RF and SVM algorithms -both widely recognized for their classification performance- were used for analysis. To evaluate classification performance, various metrics were employed, including overall accuracy, kappa statistics, F1-score, specificity and the McNemar test, all derived from confusion matrices. Using only the MS bands, RF achieved on OA of 73.75%, while SVM achieved 68.75%. When vegetation indices were included, OA increased to 82.92% for RF and 74.17% for SVM. Incorporating Gabor textures further raised the accuracy to 93.75% with RF and 80.83% with SVM. The combined use of Gabor texture features and vegetation indices improved classification performance by up to 20% for RF and 12% for SVM. Moreover, adding object height information resulted in a further

increase10% for RF and 11% for SVM. These finding underscore the importance of integrating additional features—such as texture, vegetation indices, and object height—alongside spectral information for precise crop detection from a single-date image. Furthermore, they also highlight the role of innovative data sources and machine learning techniques in improving classification accuracy and effectiveness. Notably, no similar study has been conducted in Erzincan, despite agricultural importance of the crops analysed in this research. Therefore, the outcomes of this study represent a significant step toward more accurate agricultural policy implementation and crop monitoring in the region.

Future work will aim to enhance crop classification by incorporating multi-temporal imagery and object-based image analysis, thereby building on the methods and insights presented in this study. Additionally, potential operational applications, such as annual vineyard censuses by provincial agricultural directorates, and advanced methods like transformer-based classifiers will be explored.

Author Declarations

Authors' contributions: Concept: Ö.A., Design: Ö.A., Data collection: A.A, and H.F.B., Analysis: A.A and Ö.A., Writing: Ö.A, A.A. and H.F.B.

Conflict of interest/Competing interests: The author(s) declare no conflict of interest.

Ethics approval/declarations: No need/ Not applicable.

Funding: This research received no external funding.

Consent to participate: No need/ Not applicable.

Consent for publication: No need/ Not applicable.

Data availability: Data are available on request due to privacy or other restrictions.

References

Akar A (2022). Improving the accuracy of random forest-based land-use classification using fused images and digital surface models produced via different interpolation methods. *Concurrency Computat Pract Exper* 34(6): e6787. https://doi.org/10.1002/cpe.6787

Akar O & Tunc Gormus E (2021). Land use/land cover mapping from airborne hyperspectral images with machine learning algorithms and contextual information. *Geocarto International* 37(14): 3963–3990. https://doi.org/10.1080/10106049.2021.1945149

Akar Ö, Saralıoğlu E, Güngör O & Bayata H F (2021). Determination of vineyards with support vector machine and deep learning-based image classification. 17 November 3rd Intercontinental Geoinformation Days (IGD), Mersin, Turkey

Akar Ö & Güngör O (2015). Integrating multiple texture methods and NDVI to the random forest classification algorithm to detect tea and hazelnut plantation areas in northeast Turkey. *Int J Remote Sens* 36(2): 442–464. https://doi.org/10.1080/01431161.2014.995276

Akar Ö & Güngör O (2012). Classification of multispectral images using Random Forest algorithm. Journal of Geodesy and Geoinformation 1(2): 105–112

Alzhanov A & Nugumanova A (2024). Crop classification using UAV multispectral images with gray-level co-occurrence matrix features. *Procedia Comput. Sci.* 231: 734-739. https://doi.org/10.1016/j.procs.2023.12.145

Amini S, Saber M, Rabiei-Dastjerdi H & Homayouni S (2022). Urban land use and land cover change analysis using random forest classification of landsat time series. *Remote Sensing* 14(11): 2654. https://doi.org/10.3390/rs14112654

Archer K J & Kimes R V (2008). Empirical characterization of random forest variable importance measures. Computational statistics & data analysis 52(4): 2249-2260.https://doi.org/10.1016/j.csda.2007.08.015

Atik Ş Ö (2025). Classification of Urban Vegetation Utilizing Spectral Indices and DEM with Ensemble Machine Learning Methods. International Journal of Environment and Geoinformatics 12(1): 43-53. https://doi.org/10.26650/ijegeo. 1640878

Awad M & Khanna R (2015). Support vector machines for classification. in: efficient learning machines. Apress, Berkeley, CA. https://doi.org/10.1007/978-1-4302-5990-9_3

Bareth G & Hütt C (2023). Evaluation of Direct RTK-georeferenced UAV Images for crop and pasture monitoring using polygon grids. *PFG – Journal of Photogrammetry, Remote Sensing and Geoinformation Science* 91: 471–483. https://doi.org/10.1007/s41064-023-00259-7

Bendig J, Bolten A, Bennertz S, Broscheit J, Eichhorn K & Bareth G (2014). Estimating biomass of barley using crop surface models (CSMs) derived from UAV-based RGB imaging. *Remote Sensing* 6(11):10395-10412. https://doi.org/10.3390/rs61110395

Breiman L (1999). Random forests—random features. Technical Report 567, Statistics Department, University of California, Berkeley. Retrived March 10, 2024. https://www.stat.berkeley.edu/~breiman/random-forests.pdf

Breiman L (2001). Random Forests, Machine learning, Kluwer Academic Publishers 45(1): 5-32

Breiman L (2002). Manual on Setting Up, Using, and Understanding Random Forests V3.1. Retrived June 17, 2024. https://www.stat.berkeley.edu/~breiman/Using_random_forests_V3.1.pdf

Broge N H & Leblanc E (2001). Comparing prediction power and stability of broadband and hyperspectral vegetation indices for estimation of green leaf area index and canopy chlorophyll density, *Remote Sens. Environ* 7: 156–172. https://doi.org/10.1016/S0034-4257(00)00197-8

Chen J M (1996). Evaluation of vegetation indices and a modified simple ratio for Boreal applications, *Can. J. Remote Sens.* 22: 229–242. https://doi.org/10.1080/07038992.1996.10855178

Congalton R G & Green K (1999). Assessing the accuracy of remotely sensed data: principles and practices. Boca Raton: Lewis Publishers

Congalton R G (2001). Accuracy assessment and validation of remotely sensed and other spatial information. *Int J Wildland Fire* 10: 321–328.10.1071/WF01031

Datt B (1999). VIible/near infrared reflectance and chlorophyll concentration in eucalyptus leaves. *Int. J. Remote Sens* 20: 2741–2759. https://doi.org/10.1080/014311699211778

Daughtry C S, Walthall C, Kim M, de Colstoun E B & McMurtrey J (2000). Estimating corn leaf chlorophyll concentration from leaf and canopy reflectance. *Remote Sens. Environ* 74: 229–239. https://doi.org/10.1016/S0034-4257(00)00113-9

Debnath L (2002). Wavelet Transforms and Their Applications, Springer science+, Busines media LLC, Newyork, 2002 edition, ISBN-10: 0817642048.

Deng H, Zhang W, Zheng X & Zhang H (2024). Crop classification combining object-oriented method and random forest model using unmanned aerial vehicle (UAV) multispectral image. *Agriculture* 14(4): 548. https://doi.org/10.3390/agriculture14040548

Devi R & Kaur H (2023). Automated approach to classification of crops using SVM and neural network. *Journal of Data Acquisition and Processing* 38(3): 2092-2106. DOI: 10.5281/zenodo.98549465

Domingues T, Brandão T & Ferreira J C (2022). Machine learning for detection and prediction of crop diseases and pests: A comprehensive survey. *Agriculture 12*(9):1350. https://doi.org/10.3390/agriculture12091350

dos Santos D S, Ribeiro P G, Andrade R, Silva S H G, Gastauer M, Caldeira C F, Guedes R S, Dias Y N, Filho P W M S & Ramos S J (2024). Clean and accurate soil quality monitoring in mining areas under environmental rehabilitation in the Eastern Brazilian Amazon. *Environ Monit Assess* 196*:* 385. https://doi.org/10.1007/s10661-024-12495-4

Ehammer A, Fritsch S, Conrad C, Lamers J & Dech S (2010). Statistical derivation of fPAR and LAI for irrigated cotton and rice in arid Uzbekistan by combining multi-temporal RapidEye data and ground measurements. Proc.SPIE 7824. https://doi.org/10.1117/12.864796

Faqe Ibrahim G R, Rasul A & Abdullah H (2023). Improving crop classification accuracy with integrated Sentinel-1 and Sentinel-2 data: A case study of barley and wheat. *Journal of Geovisualization and Spatial Analysis* 7: 22. https://doi.org/10.1007/s41651-023-00152-2

Feng A, Zhou J, Vories E D, Sudduth K A & Zhang M (2020). Yield estimation in cotton using UAV-based multi-sensor imagery. *Biosystems Engineering* 193: 101-114. https://doi.org/10.1016/j.biosystemseng.2020.02.014

Foody G M (2004). Thematic map comparison. *Photogramm Eng Remote Sensing 70*(5): 627–633. https://doi.org/10.14358/PERS.70.5.627

Gatera A, Kuradusenge M, Bajpai G, Mikeka C & Shrivastava S (2023). Comparison of random forest and support vector machine regression models for forecasting road accidents. *Sci African 21*, e01739. https://doi.org/10.1016/j.sciaf.2023.e01739

Gitelson A A & Merzlyak M N (1997). Remote estimation of chlorophyll content in higher plant leaves. *International Journal of Remote Sensing* 18(12): 2691–2697. https://doi.org/10.1080/014311697217558

Haboudane D, Miller J R, Pattey E, Zarco-Tejada P J & Strachan I B (2004). Hyperspectral vegetation indices and novel algorithms for predicting green LAI of crop canopies: Modeling and validation in the context of precision agriculture. *Remote Sensing of Environment* 90(3): 337-352. https://doi.org/10.1016/j.rse.2003.12.01

Hamamoto Y, Uchimura S, Watanabe M, Yasuda T, Mitani Y & Tomita S (1998). A Gabor filter based method for recognizing handwritten numerals. *Pattern Recognition* 31(4): 395–400. https://doi.org/10.1016/S0031-3203(97)00057-5

Hayli S (2002). Erzincan ovasında tarımın başlıca özellikleri. *Journal of Social Science* 1: 1-30

He S, Peng P, Chen Y & Wang X (2022). Multi-crop classification using feature selection-coupled machine learning classifiers based on spectral, textural and environmental features. *Remote Sensing* 14(13): 3153. https://doi.org/10.3390/rs14133153

Huete A, Didan K, Miura T, Rodriguez E, Gao X & Ferreira L (2002). Overview of the radiometric and biophysical performance of the MODIS vegetation indices. *Remote Sens. Environ* 83: 195–213. https://doi.org/10.1016/S0034-4257(02)00096-2

Iranzad R & Liu X (2024). A review of random forest-based feature selection methods for data science education and applications. *Int J Data Sci and Anal*. https://doi.org/10.1007/s41060-024-00509-w

Jordan C F (1969). Derivation of leaf-area index from quality of light on the forest floor, *Ecology* 50: 663–666

Kavitha S S & Kaulgud N (2024). Quantum machine learning for support vector machine classification. *Evol. Intel.* 17: 819–828. https://doi.org/10.1007/s12065-022-00756-5

Kross A, McNairn H, Lapen D, Sunohara M & Champagne C (2015). Assessment of RapidEye vegetation indices for estimation of leaf area index and biomass in corn and soybean crops. *International Journal of Applied Earth Observation and Geoinformation* 34: 235-248. https://doi.org/10.1016/j.jag.2014.08.002

Kumar P, Prasad R, Choudhary A, Mishra V N, Gupta D K & Srivastava P K (2016). A statistical significance of differences in classification accuracy of crop types using different classification algorithms. *Geocarto International* 32(2): 206–224. https://doi.org/10.1080/10106049.2015.1132483

Kwak G H & Park N W (2019). Impact of texture information on crop classification with machine learning and UAV images. Applied Sciences 9(4): 643. https://doi.org/10.3390/app9040643

Lee W S, Alchanatis V, Yang C, Hirafuji M, Moshou D & Li C (2010). Sensing technologies for precision specialty crop production. *Comput Electron Agric* 74(2): 33. https://doi.org/10.1016/j.compag.2010.08.005

Li M, Zang S, Zhang B, Li S & Wu C (2014). A review of remote sensing image classification techniques: The role of spatio-contextual information. European Journal of Remote Sensing 47(1): 389-411. https://doi.org/10.5721/EuJRS20144723

Lillesand T M, Kiefer R W & Chipman J W (2004). *Remote sensing and image interpretation*. Wiley, United States of America, pp. 552-572.

Lucena F, Breunig F M & Kux H (2022). The combined use of UAV-based RGB and DEM images for the detection and delineation of orange tree crowns with Mask R-CNN: An approach of labeling and unified framework. Future Internet 14(10): 275. https://doi.org/10.3390/fi14100275

Maes W H & Steppe K (2019). Perspectives for remote sensing with unmanned aerial vehicles in precision agriculture. *Trends in Plant Science 24*(2): 152-164. https://doi.org/10.1016/j.tplants.2018.11.007

Manzali Y & Elfar M (2023). Random forest pruning techniques: A recent review. *Oper. Res. Forum* 4: 43. https://doi.org/10.1007/s43069-023-00223-6

Marcone A, Impollonia G, Croci M, Blandinières H, Pellegrini N & Amaducci S (2024). Garlic yield monitoring using vegetation indices and texture features derived from UAV multispectral imagery. *Smart Agricultural Technology* 8: 100513. https://doi.org/10.1016/j.atech.2024.100513

Mather P M & Tso B (2009). Classification methods for remotely sensed data, Second Editon, CRC Press, United States of America.

Mather P M (2004). Computer Processing of Remotely-Sensed Images: An Introduction, Third edition, Wiley, USA, ISBN 0-470-84918-5.

Moreno-Revelo M Y, Guachi-Guachi L, Gómez-Mendoza J B, Revelo-Fuelagán J & Peluffo-Ordóñez D H (2021). Enhanced convolutional-neural-network architecture for crop classification. *Applied Sciences* 11(9): 4292. https://doi.org/10.3390/app11094292

Nidamanuri R R (2024). Deep learning-based prediction of plant height and crown area of vegetable crops using LiDAR point cloud. *Scientific Reports* 14(1): 14903. https://doi.org/10.1038/s41598-024-65322-8

Pal M (2005). Random forest classifier for remote sensing classification. *International Journal of Remote Sensing 26*(1): 217-222. https://doi.org/10.1080/01431160412331269698

Parashar D, Kumar A, Palni S, Pandey A, Singh A & Singh A P (2024). Use of machine learning-based classification algorithms in the monitoring of land use and land cover practices in a hilly terrain. *Environ Monit Assess* 196: 8. https://doi.org/10.1007/s10661-023-12131-7

Pearson R L & Miller L D (1972). Remote mapping of standing crop biomass for estimation of the productivity of the shortgrass prairie, Pawnee National Grasslands, Colorado. In Proceedings of the Eighth International Symposium on Remote Sensing of Environment Dept (pp. 1357-1381). Fort Collins, Colorado.

Pei S, Dai Y, Bai Z, Li Z, Zhang F, Yin F & Fan J (2024). Improved estimation of canopy water status in cotton using vegetation indices along with textural information from UAV-based multispectral images. Computers and Electronics in Agriculture 224, 109176. https://doi.org/10.1016/j.compag.2024.109176

Peña-Barragán J M, Ngugi M K, Plant R E & J Six J (2011). Object-based crop identification using multiple vegetation indices, textural features and crop phenology. *Remote Sens. Environ* 115(6). https://doi.org/10.1016/j.rse.2011.01.009

Penuelas J, Baret F, & Filella I (1995). Semi-empirical indices to assess carotenoids/chlorophyll-a ratio from leaf spectral reflectance. *Photosynthetica 31*(2): 221–230.

Petkov N & Wieling M B (2008). Gabor filter for image processing and computer vision, University of Groningen, Department of Computing Science, Intelligent Systems, Retrieved March, 12, 2024. http://matlabserver.cs.rug.nl/edgedetectionweb/web/ edgedetection_params.html

Pipatsitee P, Tisarum R, Taota K, Samphumphuang T, Eiumnoh A, Singh H P & Cha-um S (2023). Effectiveness of vegetation indices and UAV-multispectral imageries in assessing the response of hybrid maize (Zea mays L.) to water deficit stress under field environment. *Environ Monit Assess* 195, 128. https://doi.org/10.1007/s10661-022-10766-6

Pontius R G & Millones M (2011). Death to kappa: birth of quantity disagreement and allocation disagreement for accuracy assessment. I*nternational Journal of Remote Sensing* 32: 4407-4429. https://doi.org/10.1080/01431161.2011.552923

Potgieter A B, Zhao Y, Zarco-Tejada P J, Chenu K, Zhang Y, Porker K, Biddulph B, Dang Y P, Neale T, Roosta F & Chapman S (2021). Evolution and application of digital technologies to predict crop type and crop phenology in agriculture. *In Silico Plants* 3(1). https://doi.org/10.1093/insilicoplants/diab017

Pun Magar L, Sandifer J, Khatri D, Poudel S, Kc S, Gyawali B & Chiluwal A (2025). Plant height measurement using UAV-based aerial RGB and LiDAR images in soybean. *Frontiers in Plant Scienc*, 16, 1488760. https://doi.org/10.3389/fpls.2025.1488760

Qi J, Chehbouni A, Huete A R, Kerr Y H & Sorooshian S (1994). A modified soil adjusted vegetation index. *Remote Sens. Environ* 48: 119-126. https://doi.org/10.1016/0034-4257(94)90134-1

Rissanen K, Martin-Guay M O, Riopel-Bouvier A S & Paquette A (2019). Light interception in experimental forests affected by tree diversity and structural complexity of dominant canopy. *Agricultural and Forest Meteorology* 278: 107655. https://doi.org/10.1016/j.agrformet.2019.107655

Rodriguez-Galiano V F, Ghimire B, Rogan J, Chica-Olmo M & Rigol-Sanchez J P (2012). An assessment of the effectiveness of a random forest classifier for land-cover classification. *ISPRS Journal of Photogrammetry and Remote Sensing* 67: 93–104. https://doi.org/10.1016/j.isprsjprs.2011.11.002

Rondeaux G, Steven M & Baret F (1996). Optimization of soil-adjusted vegetation indices, *Remote Sens. Environ.* 55: 95–107. https://doi.org/10.1016/0034-4257(95)00186-7

Sah S S, Maulud K N A, Sharil S, Karim O A & Pradhan B (2023). Monitoring of three stages of paddy growth using multispectral vegetation index derived from UAV images. *The Egyptian Journal of Remote Sensing and Space Sciences* 26(4): 989-998. https://doi.org/10.1016/j.ejrs.2023.11.005

Saleem M H, Potgieter J & Arif K M (2021). Automation in agriculture by machine and deep learning techniques: a review of recent developments. *Precision Agric* 22: 2053–2091. https://doi.org/10.1007/s11119-021-09806-x

SenseFly (2022). eBee SQ the advanced agricultural drone. Retrieved July 2024. https://srv.jgc.gr/Pdf_files/eBee-SQ-en.pdf

Shahi T B, Xu C Y, Neupane A & Guo W (2022). Machine learning methods for precision agriculture with UAV imagery: A review. *Electron. Res. Arch* 30(12): 4277–4317. doi: 10.3934/era.2022218

Sims D A & Gamon J A (2002). Relationships between leaf pigment concentration and spectral reflectance across a wide range of species, leaf structures and developmental stages. *Remote Sens. Environ* 81: 337–354 https://doi.org/10.1016/S0034-4257(02)00010-X

Singh R & Kumar V (2023). Evaluating automated endmember extraction for classifying hyperspectral data and deriving spectral parameters for monitoring forest vegetation health. *Environ Monit Assess* 195: 72. https://doi.org/10.1007/s10661-022-10576-w

Song B & Park K (2020). Detection of aquatic plants using multispectral UAV imagery and vegetation index. *Remote Sensing 12*(3): 387. https://doi.org/10.3390/rs12030387

Teimouri M, Mokhtarzade M, Baghdadi N & Heipke C (2023). Generating virtual training labels for crop classification from fused Sentinel-1 and Sentinel-2 time series. *PFG – Journal of Photogrammetry, Remote Sensing and Geoinformation Science* 91: 413–423. https://doi.org/10.1007/s41064-023-00256-w

Tetteh G O, Schwieder M, Erasmi S, Conrad C & Gocth A (2023). Comparison of an optimised multiresolution segmentation approach with deep neural networks for delineating agricultural fields from Sentinel-2 images. *PFG – Journal of Photogrammetry, Remote Sensing and Geoinformation Science* 91: 295–312. https://doi.org/10.1007/s41064-023-00247-x

TR Erzincan Governorate (2024). http://www.erzincan.gov.tr/erzincan-uzumu (Retrieved March, 12, 2024).

Tzotsos A & Argialas D (2008). Support vector machine classification for object-based image analysis. In: Blaschke, T., Lang, S., Hay, G.J. (eds) Object-Based Image Analysis. Lecture Notes in Geoinformation and Cartography. Springer, Berlin, Heidelberg. https://doi.org/10.1007/978-3-540-77058-9_36

Vapnik V N (1998). Statistical Learning Theory. New York: Wiley.

Wan L, Li Y, Cen H, Zhu J, Yin W, Wu W, Zhu H, Sun D, Zhou W & He Y (2018). Combining UAV-based vegetation indices and image classification to estimate flower number in oilseed rape. *Remote Sensing 10*(9):1484. https://doi.org/10.3390/rs10091484

Watts J D, Powell S L, Lawrence R L & Hilker T (2011). Improved classification of conservation tillage adoption using high temporal and synthetic satellite imagery. *Remote Sensing of Environment* 115(1): 66–75. https://doi.org/10.1016/j.rse.2010.08.005

Wu Q, Zhang Y, Zhao Z, Xie M & Hou D (2023). Estimation of relative chlorophyll content in spring wheat based on multi-temporal UAV remote sensing. *Agronomy* 13(1): 211. https://doi.org/10.3390/agronomy13010211

Xu Q, Jin M & Guo P (2022). A high-precision crop classification method based on time-series UAV images. Agriculture 13(1): 97. https://doi.org/10.3390/agriculture13010097

Yao L, Shono Y, Nowinski C, Dworak E M, Kaat A, Chen S, Lovett T, Ho E, Curtis L, Wolf M, Gershon R & Benavente J Y (2024). Prediction of cognitive impairment using higher order item response theory and machine learning models. *Frontiers in psychiatry* 14, 1297952. https://doi.org/10.3389/fpsyt.2023.1297952

Yi Z, Jia L & Chen Q (2020). Crop classification using multi-temporal Sentinel-2 data in the Shiyang river basin of China. *Remote Sensing 12*(24): 4052. https://doi.org/10.3390/rs12244052

Zermane A, Mohd Tohir M Z, Zermane H, Baharudin M R & Mohamed Yusoff H (2023). Predicting fatal fall from heights accidents using random forest classification machine learning model. *Safety Science* 159, Article 106023. https://doi.org/10.1016/j.ssci.2022.106023

Zhang J, Pan Y, Tao X, Wang B, Cao Q, Tian Y, Zhu Y, Cao W & Liu X (2023). In-season mapping of rice yield potential at jointing stage using Sentinel-2 images integrated with high-precision UAS data. *European Journal of Agronomy* 146, 126808. https://doi.org/10.1016/j.eja.2023.126808

Zhang J, Qiu X, Wu Y, Zhu Y, Cao Q, Liu X & Cao W (2021b). Combining texture, color, and vegetation indices from fixed-wing UAS imagery to estimate wheat growth parameters using multivariate regression methods. *Computers and Electronics in Agriculture* 185, 106138. https://doi.org/10.1016/j.compag.2021.106138

Zhang X, Sun Y, Shang K, Zhang L & S Wang (2016). Crop classification based on feature band set construction and object-oriented approach using hyperspectral images. *IEEE Journal of Selected Topics in Applied Earth Observations and Remote Sensing* 9(9): 4117-4128. doi: 10.1109/JSTARS.2016.2577339.

Zhang H, Wang Y, Shang J, Liu M & Li Q (2021a). Investigating the impact of classification features and classifiers on crop mapping performance in heterogeneous agricultural landscapes *Int. J. Appl. Earth Obs. Geoinf* 102, 102388. https://doi.org/10.1016/j.jag.2021.102388

Zou M, Liu Y, Fu M, Li C, Zhou Z, Meng, H & Ren Y (2024). Combining spectral and texture feature of UAV image with plant height to improve LAI estimation of winter wheat at jointing stage. *Frontiers in Plant Science*, 14, 1272049 https://doi.org/10.3389/fpls.2023.1272049